

# FEMAP and NX NASTRAN Modal Analysis of Unswept and Swept Wings

Santiago Ulloa\*, Kiril Yampolsky†, Logan Resendez‡, Cameron Whitfield§, and Mark A. Nuguid¶  
*San Diego State University, San Diego, CA, 92182*

The following paper is an exploration of the natural frequencies and associated modes of three-dimensional wing geometries of a straight-wing box structure and a similar swept-wing box structure and their varying internal structures. The models are created in FEMAP and analyzed using NX NASTRAN with each wing box model run through a convergence test to adequately identify a reasonable finite element model mesh resolution for analysis and further comparison between the varying geometries. Additionally, the internal structure of all geometries was varied for each swept and unswept wing geometry to further analyze and compare varying wing rib placements and the effect on natural frequency and mode shapes. By analyzing the wing-box structure, with and without certain ribs, we can visually see the effect of hysteretic damping due to the addition of ribs. This study aimed to present results from a theoretical dynamic analysis of varying three-dimensional wing box structures for exploratory and educational purposes.

## I. Nomenclature

$\theta$	=	Angle of Ribs From Leading Edge
$\Delta_{LE}$	=	Leading Edge Sweep
$E$	=	Young's Modulus of Elasticity
$\nu$	=	Poisson's Ratio
$\rho$	=	Density
$t_1$	=	Thickness of Ribs

## II. Introduction

In this report, we were tasked with analyzing three different wing boxes whose internal structures consisted of four ribs. The first wing is unswept, the second wing has a 30-degree wing sweep with the ribs parallel to free-stream flow, and the final wing box is a 30-degree swept wing with the ribs perpendicular to the leading edge of the wing box. We will be analyzing these structures in FEMAP and using modal analysis using NX NASTRAN to identify the natural frequencies, associated modes, and visualize the mode shapes of these structures and comparing our findings.

## III. Setup of the Wings and Internal Structures

### A. Straight Rectangular Wing

For the first wing geometry, we were to model a straight rectangular wing box structure with no taper or sweep. This wing geometry is the simplest of the three, with three spars going along the leading edge, trailing edge, and half-chord regions of the wing.

---

\*Student, SDSU Aerospace Engineering, 5500 Campanile Drive San Diego, CA 92182

†Student, SDSU Aerospace Engineering, 5500 Campanile Drive San Diego, CA 92182

‡Student, SDSU Aerospace Engineering, 5500 Campanile Drive San Diego, CA 92182

§Student, SDSU Aerospace Engineering, 5500 Campanile Drive San Diego, CA 92182

¶Student, SDSU Aerospace Engineering, 5500 Campanile Drive San Diego, CA 92182

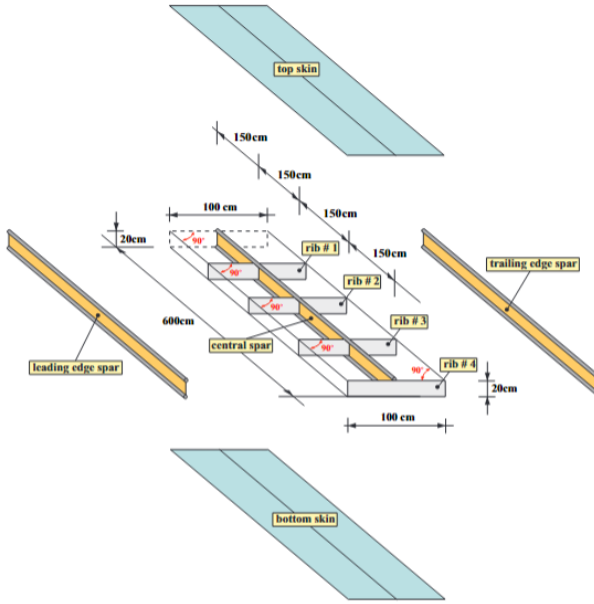


**Fig. 1 Exploded View the First Wing Structure [2]**

Furthermore, four ribs starting from the tip chord are divided evenly amongst the wing structure at 150 cm apart. Note that there is no rib at the root chord location. Similarly, the top and bottom skins are modeled as rectangular shapes along the top and bottom of the internal wing box structure. The following figure displays important dimensions for how the wing is structured. An exploded view of the wing structure including all ribs is presented in Fig. 1.

This wing structure and all of its components have the following material properties, which are be presented in Table 1. Note that these material properties carry on for the other wing geometries as well, and will be referencing this table in the other sections. All surfaces which we modeled in FEMAP to create the wing box structure did not display a thickness, the thickness of each part was included in the property definitions of each part.

Property	
Elastic Modulus, E (GPa)	72
Poisson's Ratio, $\nu$	0.3
Material Density, $\rho \frac{kg}{m^3}$	2700

**Table 1 Material Properties for the Wing Structure [1]**

The following structures have the following have respective thicknesses, which, as previously mentioned, is necessary in order to properly model each part of FEMAP. The following table contains these values:

Part	Thickness (mm)
Spar	2.5
Rib	2.0
Skin	2.0

**Table 2 Structure Thicknesses**

Note that these values hold for the other wing geometries as well, so in a similar manner to Table 1, Table 2 will be referenced in future sections.

In order to model this wing structure, we created surfaces by designating the corners of the rectangular shapes designated by the dimensions of the structure, where the origin in the (x,y,z) coordinate system is located on the trailing

edge corner of the root chord on the plane of the bottom skin.

From that point, all other coordinate points for the rectangular geometries are modeled along this origin. After doing so, the geometries will have coincident edges, where the ribs contact the skins and outer spars, as well as intersect the center spar perpendicularly. Note that meshing the geometry this way can create uneven meshing on the skin and spars. To get around this, use the 'Non manifold Add' option located in the 'Geometry -> Surface'. Doing so tells the program that these geometries are connected at their points of contact, thus creating individual edges between each point of intersection.

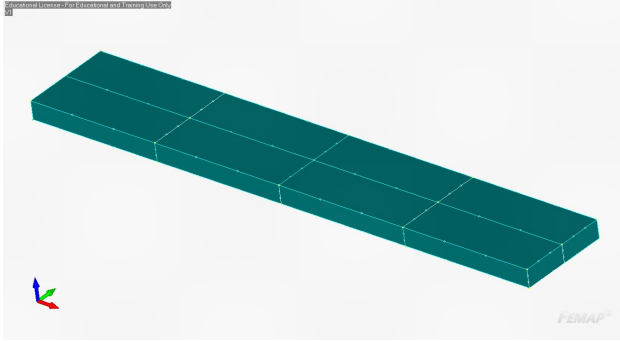


**Fig. 2 Wing 1 Original Geometry**

Meshing this geometry requires that you mesh each surface created by the intersecting lines. For example, the top skin will be divided into 8 individual surfaces, which are created by the intersections caused by the ribs with the center spar. Note that this process is used for modeling all wing geometries. The model for the first wing structure in FEMAP is presented in Fig.2.

### B. Swept Wing

The second wing geometry is similar to the first one, however, it presents with a 30-degree leading edge sweep. There is no taper, so all chord lengths along the wing remain the same, however, in the presence of the sweep, the ribs are placed at a 60-degree angle relative to the trailing edge spar. The following figure (Fig. 3) contains the dimensions for this wing configuration.

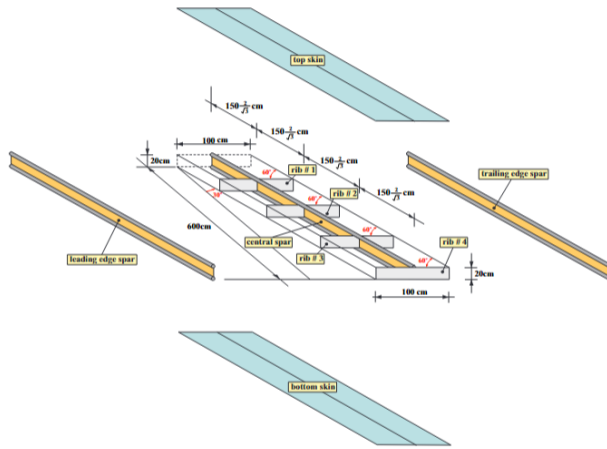


**Fig. 3 Exploded View of Second Wing Geometry [2]**

As mentioned earlier, the material properties and structural thicknesses are the same and are tabulated in Table 1 and Table 2, respectively.

The geometry was modeled on FEMAP in the exact manner mentioned in the straight rectangular wing section of this report. Below is a figure of the geometry for the swept wing.

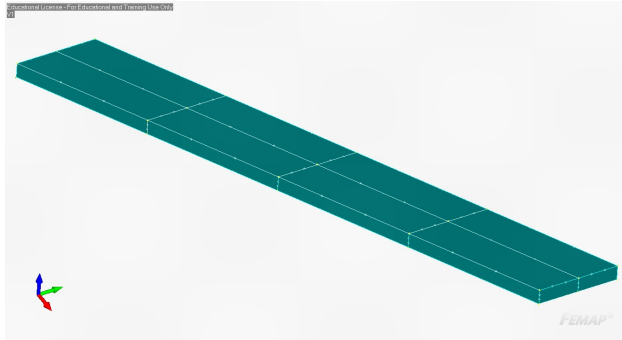


**Fig. 4** Wing 2 Original Geometry

### C. Swept Wing with Ribs Perpendicular to the Spars

The third wing geometry is similar to the second, which is the swept wing, however, the ribs on this wing geometry are perpendicular to the wing spar. Once again, this wing geometry has the same material properties and structural thicknesses tabulated in Tables 1 and 2, respectively. Figure 5 contains the dimensions for this wing configuration. Note that rib four is not perpendicular to the spars, as it must be flush with the sweep in order to close the wing off without overlap or overextending spar lengths.

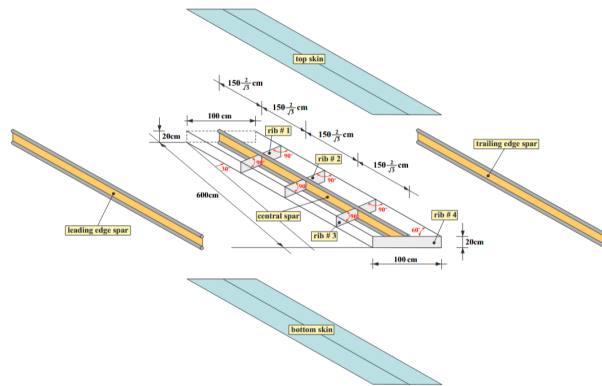


**Fig. 5** Exploded View of Third Wing Geometry [2]

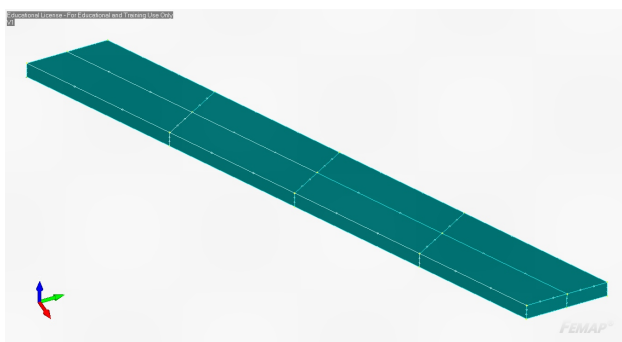


**Fig. 6** Wing 3 Original Geometry

Once again, this geometry is modeled using the same process outlined in the 'Straight Rectangular Wing' section of this paper. Figure 6 illustrates the third wing geometry and surface creation modeled on FEMAP.

#### IV. Meshing The Wing Geometries

In order to mesh the geometries, we had to define a number,  $n$ , to denote the number of nodes placed along a rib segment. Similarly, let  $n$  also denote the number of nodes along the spar segment. Due to the nature of the geometry, one rib segment consists of only half of the entire rib. Similarly, one spar segment consists of 1/4 of the entire spar length. To visualize this, refer to the following figure for the nodes as well as the process in which we created the wing geometry in the 'Straight Rectangular Wing' section. Furthermore, we used 4-noded quadrilateral (QUAD4) shell elements to create the mesh. This results in a 4 sided mesh element, with many being distributed across every surface. We check for coincident nodes to ensure that the mesh clearly defines the structure. Let pink define the top skin, yellow denote the spars, green define the ribs in these images, and blue define the bottom skin.

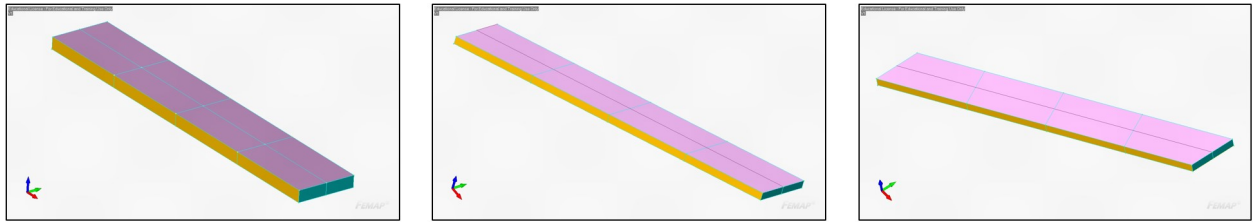


**Fig. 7** Meshed Wing Geometries of Wings 1, 2, and 3

In the above figures, there is 1 node in between the segments, and the mesh is created using the points that were created by points of intersection during the modeling of their respective geometries. Note that each surface is defined by the lines of intersection, or the spar and rib segments as defined earlier. Increasing  $n$  will increase the amount of elements over these surfaces.

##### A. Wing Convergence Without Ribs and No Imposed Boundary Conditions

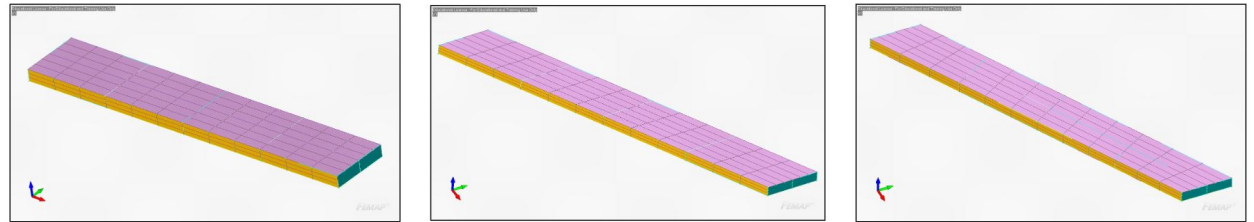


**Fig. 8** Meshed Wing Geometries

Figure 8 illustrates the outcome of our meshing process, presenting the finite plate elements modeling the various structural elements of our wing box structures. We continuously doubled the mesh and conducted our convergence tests of the wing structures without any ribs or imposed boundary conditions.

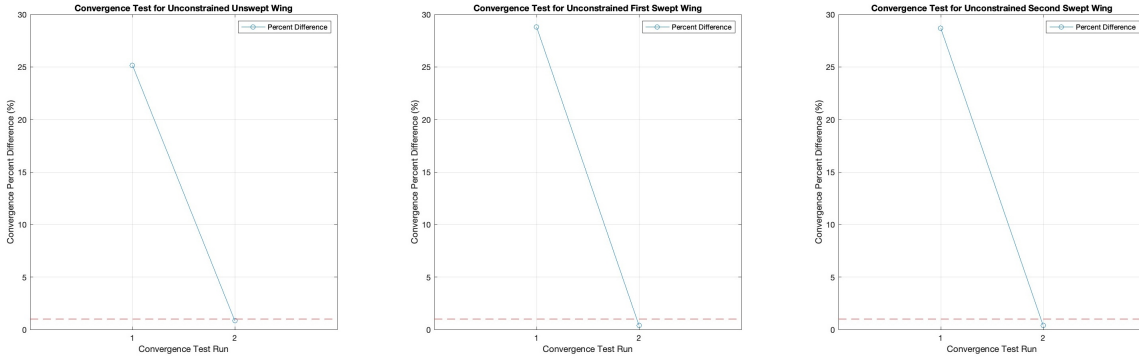


**Fig. 9 Convergence Test of Unconstrained Unswept and Swept Wings**

For all wing structures, convergence was achieved after our third iteration, the number of runs and the associated percent different for each wing is presented in Fig. 9. The converged mesh are those presented in Fig. 8. There is an inclusion of a horizontal line at 1 % in order to visualize the convergence criteria of a percent difference less than 1% for the average difference across all frequencies for all modes considered for each mesh. The following tables are the resulting modes and frequencies for the listed wing geometries and conditions.

Mode	Frequency (n=2) (Hz)	Frequency (n=3) (Hz)
1	4.06926E-5	4.0028E-5
2	2.64363E-5	3.74877E-5
3	1.51636E-5	3.62053E-5
4	2.31479E-5	2.49457E-5
5	3.12995E-5	2.37732E-5
6	3.35252E-5	2.81764E-5
7	10.0955	10.07182
8	12.43983	12.48879
9	27.2055	26.91498
10	27.85394	28.32136

**Table 3 First Wing: 10 Natural Modes and Frequencies for No Rib, No Constraint Condition**

Mode	Frequency (n=2) (Hz)	Frequency (n=3) (Hz)
1	1.72246E-5	6.84555E-5
2	2.08837E-5	5.29943E-5
3	2.5424E-5	2.89488E-5
4	2.62982E-5	2.49445E-5
5	3.44284E-5	2.602E-5
6	5.13055E-5	2.78003E-5
7	12.21224	12.18326
8	16.02875	16.095
9	23.87261	23.74134
10	26.05149	25.9392

**Table 4 Second Wing: 10 Natural Modes and Frequencies for No Rib, No Constraint Condition**

Mode	Frequency (n=2) (Hz)	Frequency (n=3) (Hz)
1	2.688E-5	6.8158E-5
2	2.34141E-5	2.95635E-5
3	1.62339E-5	2.54532E-6
4	7.72696E-6	1.47553E-5
5	2.46415E-5	2.44916E-5
6	2.77693E-5	3.8719E-5
7	12.20906	12.17815
8	16.05532	16.1002
9	23.93782	23.7784
10	26.07764	25.96442

**Table 5 Third Wing: 10 Natural Modes and Frequencies for No Rib, No Constraint Condition**

### B. Wing Convergence Without Ribs and Imposed Boundary Conditions

In Fig. 10, the nodal number,  $n$ , has been set to 1, which puts 1 node along each rib and spar segment. As a result, the mesh over one surface will result in 1 element across each respective surface. There are 8 surfaces that make up the top and bottom skin respectively, so in total, there are 8 elements across those structures.

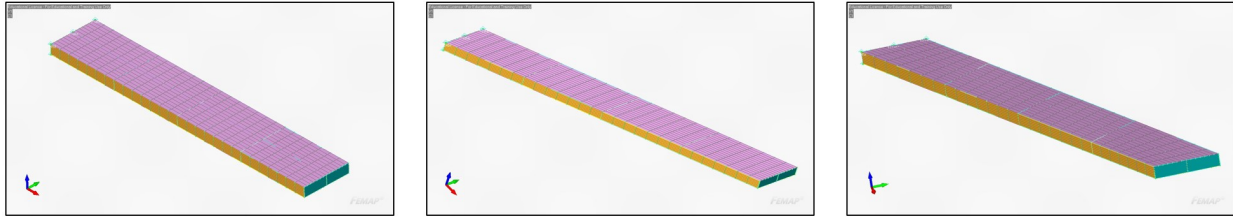


**Fig. 10 Meshed Wings 1, 2, and 3 with Imposed Boundary Conditions**

Figure 10 illustrates the converged mesh geometries for the wing structures after we imposed boundary conditions, fixing the wing at the root chord. The following illustrates the convergence tests we ran at varying mesh resolutions to arrive at our converged mesh. .

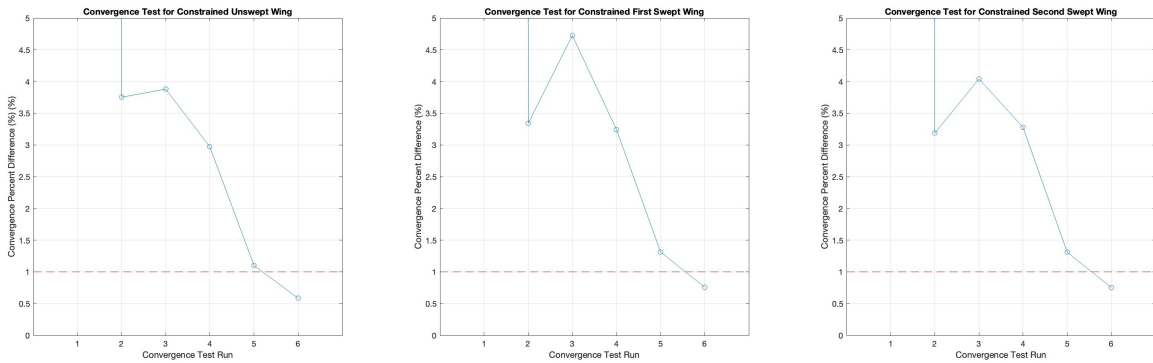


**Fig. 11 Convergence Test of Constrained Unswept and Swept Wings**

The first run percent difference was not included in the plot as it was three orders of magnitude larger than the other differences, inclusion of the value on the plot would render the following convergence test as visually indiscernible.

Additionally, there is an inclusion of a horizontal line at 1 % like the plots for the tests without boundary conditions. The following tables are the resulting modes and frequencies for the listed wing geometries and conditions.

Mode	Frequency (n=6) (Hz)	Frequency (n=7) (Hz)
1	6.611872	6.594324
2	13.06566	13.06024
3	23.20828	23.15745
4	30.72202	30.60013
5	30.76568	30.61177
6	31.92292	31.94017
7	32.05697	32.1046
8	32.286	32.38345
9	32.61871	32.78399
10	33.06701	33.31556
11	33.64618	33.98927
12	34.37446	34.817
13	35.27128	35.80923
14	36.35375	36.97254
15	37.3986	37.45245

**Table 6 First Wing: First 15 Natural Modes and Frequencies for No Rib, Clamped Constraint Condition**

Mode	Frequency (n=6) (Hz)	Frequency (n=7) (Hz)
1	4.959551	4.949234
2	15.2328	15.22735
3	15.69483	15.66641
4	27.52434	27.33083
5	30.21424	30.06685
6	41.15739	41.19527
7	41.1918	41.24524
8	41.25358	41.27967
9	41.26383	41.42307
10	41.3516	41.63148
11	41.497	41.91172
12	41.70493	42.2721
13	41.99253	42.72042
14	42.37974	43.2623
15	42.88026	43.89539

**Table 7 Second Wing: First 15 Natural Modes and Frequencies for No Rib, Clamped Constraint Condition**

Mode	Frequency (n=6) (Hz)	Frequency (n=7) (Hz)
1	4.960802	4.950135
2	15.23201	15.22677
3	15.70423	15.67386
4	27.56239	27.3579
5	30.2661	30.10727
6	41.20472	41.23008
7	41.23983	41.2521
8	41.27265	41.31406
9	41.30699	41.45962
10	41.4116	41.67016
11	41.5582	41.94807
12	41.75719	42.29935
13	42.01731	42.7286
14	42.34725	43.24024
15	42.76022	43.84098

**Table 8 Third Wing: First 15 Natural Modes and Frequencies for No Rib, Clamped Constraint Condition**

In later sections, Tables 6-8 are important in the identification of the first bending and first torsional modes.

## V. Modal Analyses of the Wing Structures

For this section, we are assigned to analyze these geometries in 6 different ways. These analyses are defined in the subsection titles.

### A. Modal Analysis of Wings With No Boundary Conditions and No Ribs

Refer to Fig. 8 to recall how this analysis was meshed. Similarly, recall tables 3-5 for the modes and frequencies for this analysis. For this analysis, we are to analyze the first 10 natural modes and frequencies of each wing structure with no boundary conditions and without the ribs meshed. Note that these results exclude the ribs and the boundary conditions at the wing root for the analysis. In these analyses, convergence occurs on the third iteration, where  $n = 3$ , and the previous iteration, where  $n = 2$ . The following figure is the mesh for the  $n = 3$  condition.

#### 1. First Six Modes

Note that for all wing geometries, the first six modes are significantly smaller than the last four modes. As a result, during the convergence tests, these first six modes would not converge, despite the last four converging after three iterations. This means that these first six modes should not be included in the analysis and are not reliable in representing the actual natural frequencies of those nodes. However, the last four nodes have converged, therefore, these can be considered to be the natural frequencies at these modes, and no further refinement of the mesh is needed. It should be noted that the first and second elastic modes are going to be the first 2 modes that have converged.

#### 2. First and Second Elastic Modes

The first and second elastic modes are representative of the first modes where convergence has occurred. In the figures below, the first image (right), depicts the wing structure displaying deformation behavior similar to that caused by pure torsion. Note that the geometry has twisted on both ends due to the lack of constraints. Similarly, the second image (left), displays the wing structure in pure bending. Similarly, note that the whole structure has bent into a V-shape. In locations where the spars are located, there is relatively little local deformation, however, the center spar has been displaced vertically by a relatively large margin with respect to the rest of the geometry.

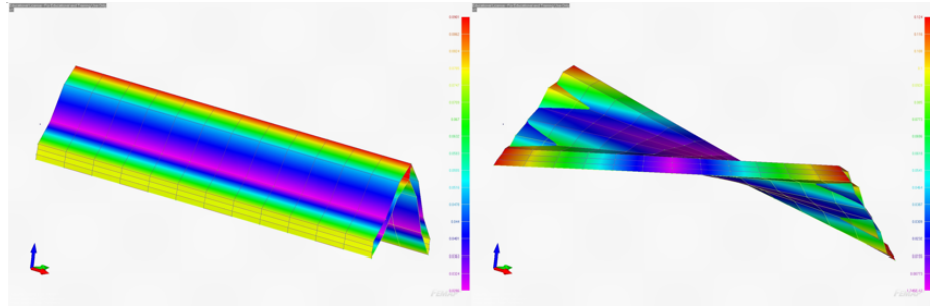


**Fig. 12 Unswept Wing First and Second Elastic Modes**

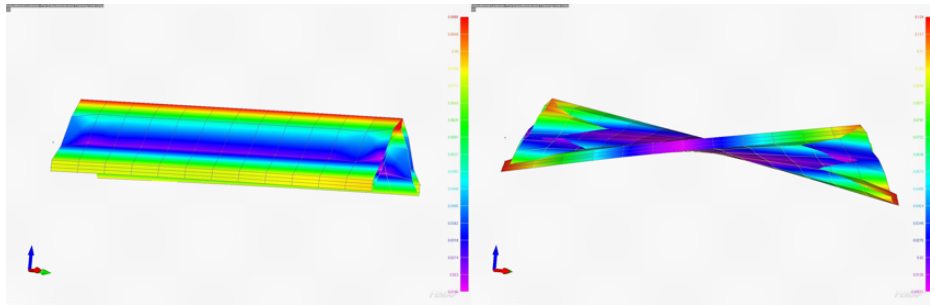


**Fig. 13 First Swept Wing First and Second Elastic Modes**

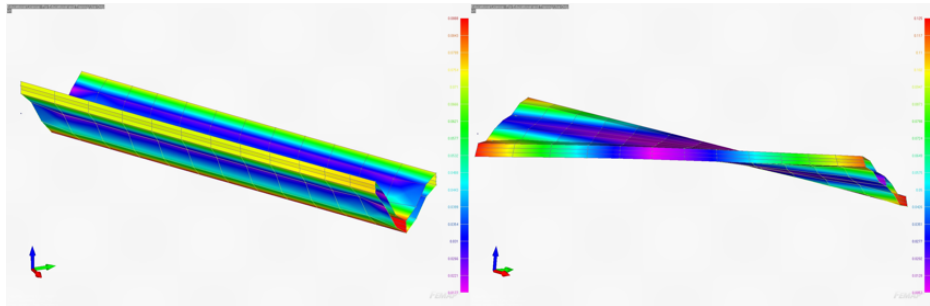


**Fig. 14 Second Swept Wing First and Second Elastic Modes**

Note that the second and third wing geometries are the same apart from the ribs, so it is sufficient to use only one swept wing geometry to represent both structures.

#### B. Modal Analysis of Wings With No Ribs and Imposed Boundary Conditions

Refer to Fig. 8 to recall how this analysis was meshed. Similarly, recall tables 6-8 for the modes and frequencies for this analysis. For this analysis, we are to analyze the first 10 natural modes and frequencies of each wing structure with clamped boundary conditions and without the ribs meshed. Similarly, note that this results in the ribs not being considered in the analysis. In these analyses, convergence occurs on the third iteration, where  $n = 6$ , and the previous iteration, where  $n = 7$ . The following figure is the mesh for the  $n = 7$  condition.

##### 1. First Six Modes

For this analysis, the first 6 modes display different behavior from that of the first analysis. The introduction of the clamped boundary condition allows the first 6 modes to not only increase in frequency significantly but also converge.

Because of this, all frequencies are the natural frequencies at those modes, and further refinement of the mesh is not necessary.

## 2. First Bending and First Torsional Modes

The first bending and torsional modes for this analysis are 1 and 2 respectively. The first image (left), displays the bending mode. Note that due to the clamped boundary condition on what is considered to be the root chord side of the wing, there is no displacement. The behavior of the deformation is similar to that of a cantilever beam that is fixed on one end, where the tip of the beam has the most displacement. Similarly, the second image (right), depicts the torsional mode. Note that the root chord end still displays no deformation. However, the tip chord of the wing has been twisted, with the trailing edge and leading edge spar on this end of the wing structure displaying the largest deformation that is equal and opposite. Also, the skin sags in the areas in between the spars, almost pinching the end shut.

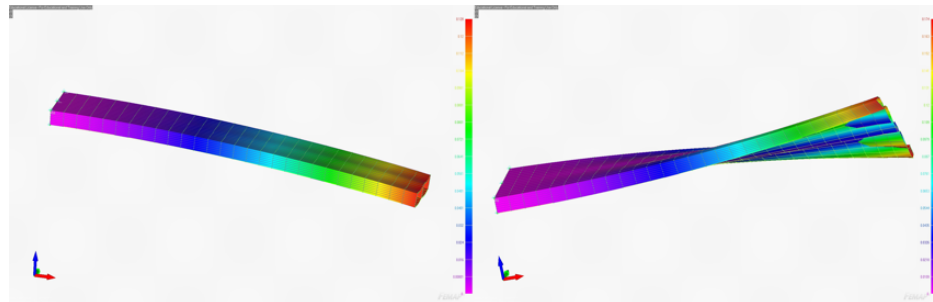


**Fig. 15 Unswept Wing First Bending and Torsion Modes**

For the swept wing geometries, the behavior of the deformation implies that these geometries are more susceptible to torsion, displaying a higher angle of twist.

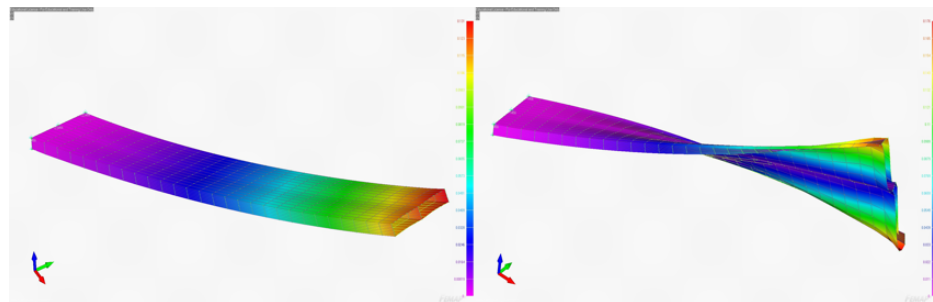


**Fig. 16 First Swept Wing First Bending and Torsion Modes**

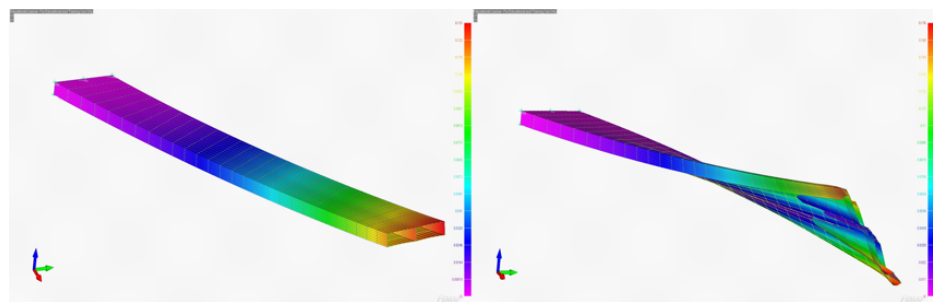


**Fig. 17 Second Swept Wing First Bending and Torsion Modes**

The second and third geometries are the same apart from the ribs, so similar to the first analysis, only one geometry

from the second or third wing structure is sufficient to represent either in this case.

### C. Modal Analysis of Wings With Rib 4 Meshed and Imposed Boundary Conditions

The modal analysis for this configuration requires that we begin to mesh the ribs, starting with rib 4, which is located at the tip chord. The clamped boundary condition remains, and the analysis is done with the mesh elements with which the convergence test holds, which was the  $n = 7$  condition. The first 15 modes for this analysis are listed in Table 9. Note there is a notable increase in the frequencies of modes that are greater than 3. Similarly, in the following images, note that the introduction of the fourth rib changes the behavior of the deformation. This is most notable in the torsional mode, where the point of max deformation is no longer located at the end of the wing, but towards the center.

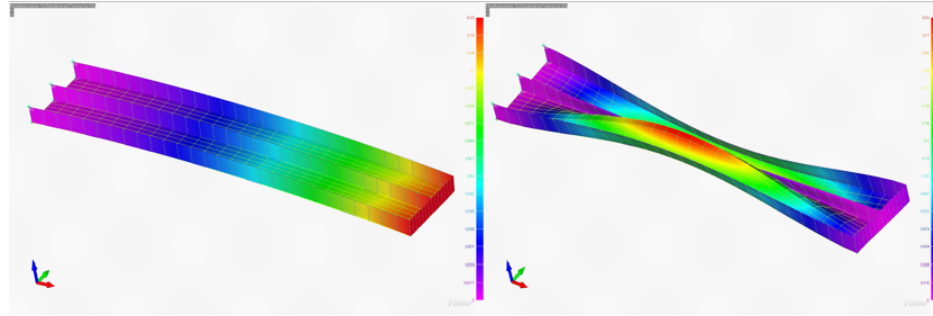


**Fig. 18 Unswept Wing With Rib 4 First Bending and Torsion Modes**

For the first swept wing, the introduction of the fourth rib has caused an uneven torsional deformation, where the maximum deformation has shifted to the leading edge spar.

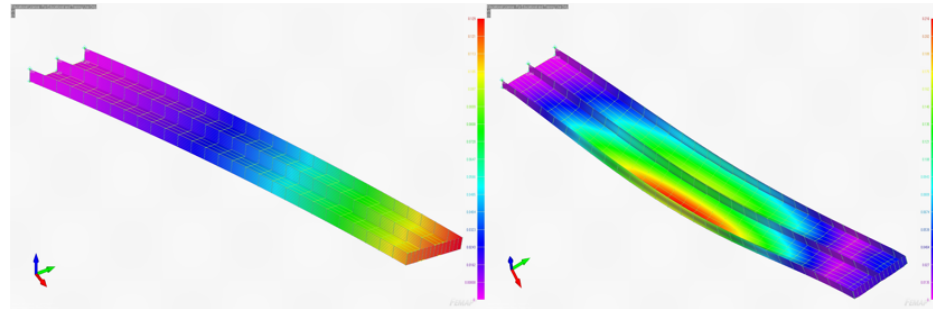


**Fig. 19 First Swept Wing With Rib 4 First Bending and Torsion Modes**

For the second swept wing, the bending moment is exactly the same as the first swept wing. This is because the wing boxes are identical when the fourth rib and the skin are the only things considered in the analysis. The only difference between the first and second swept wings is the geometries of ribs 1,2 and 3. Despite the torsional geometries looking different, they still have the maximum deformation in the same spot. Comparing the second swept wing in Figure 20, with Figure 17, it is clear that adding a rib allows the wing to maintain its shape despite having torsion acting on it.

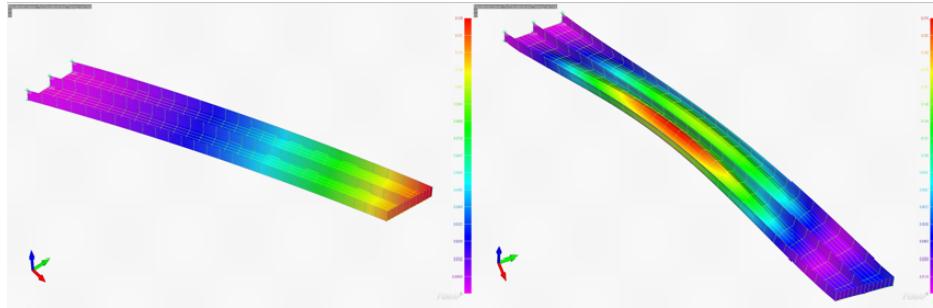


**Fig. 20 Second Swept Wing With Rib 4 First Bending and Torsion Modes**

#### D. Modal Analysis of Wings With Ribs 1 and 4 Meshed and Imposed Boundary Conditions

The modal analysis for this configuration required the mesh of ribs 1 and 4. All the same conditions were met from the previous mesh meaning the wings are still constrained, and the convergence of  $n=7$  for the mesh still remains. The locations of rib 1 can be found in Figures 1,3, and 5 for their respective wings. After meshing rib 1, a modal analysis was conducted.

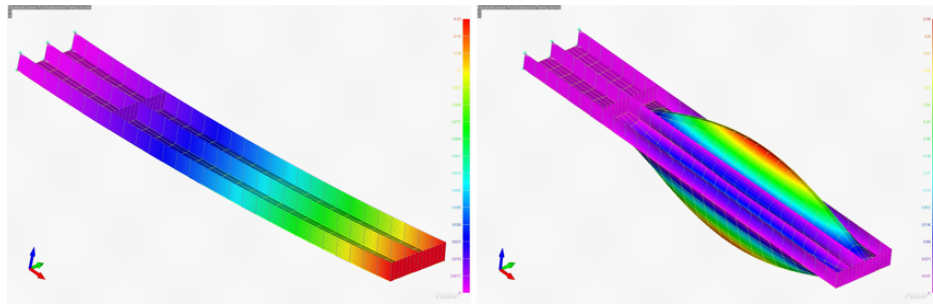


**Fig. 21 Unswept Wing With Ribs 1 and 4 First Bending and Torsion Modes**

Comparing the torsional mode seen in Figure 21, and comparing it with the torsional mode in Figure 18, it can be seen that when ribs 1 and 4 are meshed, the unswept wing is able to maintain its shape better. It can also be noted that the deformation occurs mainly on the right side when both ribs 1 and 4 are meshed in comparison to the having a more clear deformation on the left side when only rib 4 is meshed. Despite this, looking at the modal analysis, it can be seen when examining the torsional mode 2 in Table 9, there is not much difference in the frequencies. It is also important to note that the deformation moves towards the wing tip, and is no longer right in the center. This is because, with the addition of the rib, the wing tip experiences more torsion and causes more deformation closer to it. When comparing the elastic bending modes, they are very similar with most of the deformation at the tip. This shows that despite adding another rib, the elastic deformation will be very similar.

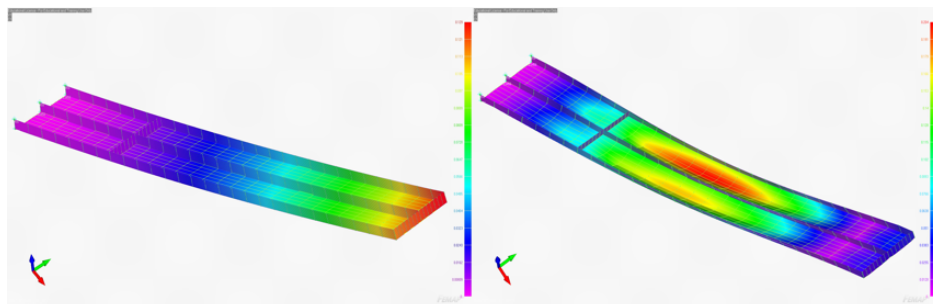


**Fig. 22 First Swept Wing With Ribs 1 and 4 First Bending and Torsion Modes**

Similar to the unswept wing, the first swept wing shows that when adding rib 1, the torsional deformation will transition from the trailing edge to the leading edge side of the wing. The modal analysis in Table 10 shows that despite this, for both the torsional mode 2 and elastic mode 1, there is a very small difference in frequencies between having ribs 1 and 4 and just having rib 4. The elastic deformation is also visually very similar with the largest deformation happening at the wing tip and the smallest happening at the wing root.

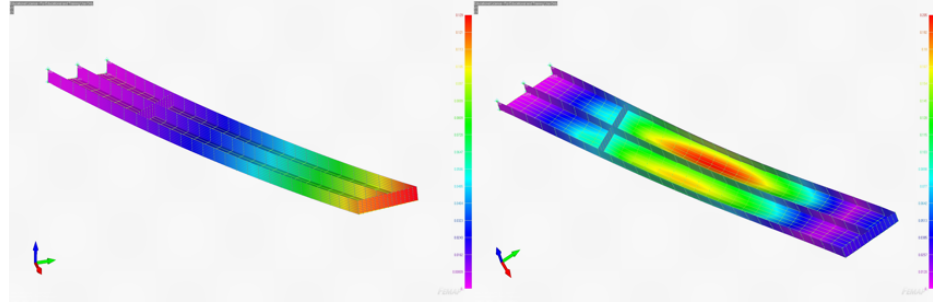


**Fig. 23 Second Swept Wing With Ribs 1 and 4 First Bending and Torsion Modes**

The second swept wing also keeps the pattern that is seen with the first swept wing. Looking at the torsional analysis between figure 20, and figure 23. The main deformation shifts from the left side of the wing to the right side. The elastic deformation remains very similar as the tip of both having ribs 1 and 4 meshed and just having rib 4 meshed is where the max deformation occurs, and moving towards the root, the deformation lessens. When comparing Figures 21, 22, and 23, they all have very similar bending deformations, and the movement is about the same. This shows that the shape of the wings, and the implementation of rib 4 do not affect the bending deformation that much. On the other hand, there is a clear difference in the torsional deformation between the unswept wing and the two swept wings. The unswept wing keeps its shape, while the two swept wings experience torsional bending. The locations of the deformations remain in the same spots.

#### E. Modal Analysis of Wings With Ribs 1, 2, and 4 Meshed and Imposed Boundary Conditions

For this modal analysis, in addition to meshed ribs 1 and 4, rib 2 was meshed as well. The location of rib 2 can be found in Figures 1,3 and 5 for their respective wings. Everything else remains the same, the only difference is that rib 2 is now meshed.

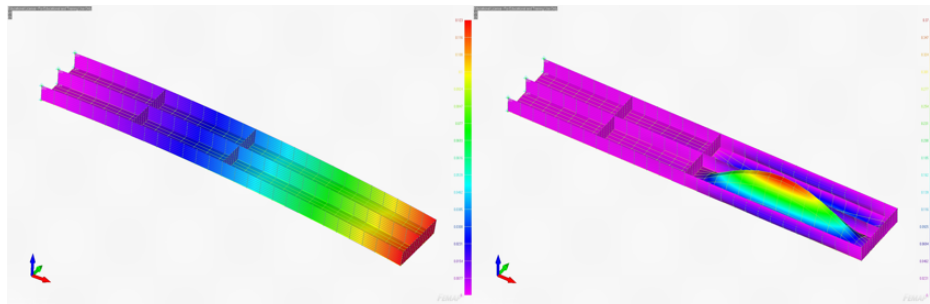


**Fig. 24 Unswept Wing With Ribs 1, 2, and 4 First Bending and Torsion Modes**

Comparing Figure 21 with Figure 24, it is seen that the torsional deformation has moved from the leading edge to the trailing edge side. It can also be seen that with the addition of rib 2, the torsional deformation moves closer to the tip, and there is very little torsional deformation between the root of the wing and rib 2. The bending mode on the other hand is still very similar to the unswept bending with only ribs 1 and 4, which further shows that the bending deformation is not affected by the addition of ribs for unswept wings. In Table 9, the modal analysis can be seen to not change much between the previously ribbed iteration and this one.

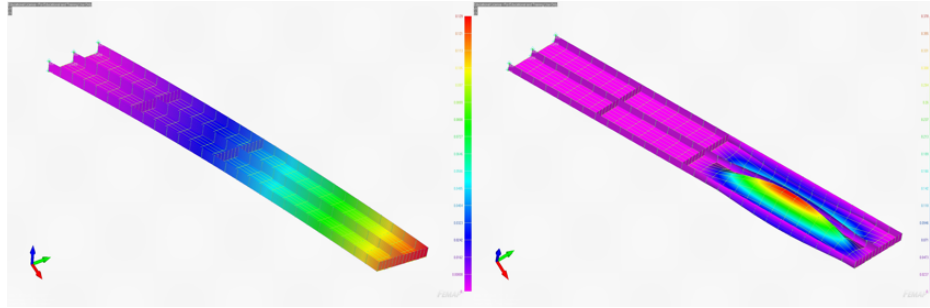


**Fig. 25 First Swept Wing With Ribs 1, 2, and 4 First Bending and Torsion Modes**

The first swept wing shown above in Figure 25 has a torsional deformation that mainly takes place near the trailing edge side of the tip. With the addition of meshed rib 2, comparing it to Figure 22, the deformation moves closer to the tip and only affects the region between the tip and meshed rib 2. The pattern clearly shows that the addition of ribs stabilizes the wing as it does not have much bend compared to Figure 22. This supports the idea that the addition of ribs stabilizes the wing and helps it become resistant to torsional deformation. When comparing the bending deformation between the first swept wing in Figure 25 and Figure 22, there is not much difference. The maximum bending occurs near the tip for both and the wing gets less affected by it the closer to the fixed boundary condition. This shows that the additions of ribs will mostly impact the torsional movement of the wing but not bending. When looking at the modal analysis in Table 10, the difference between the swept wing having ribs 1 and 4 in comparison to the wing having ribs 1,2 and 4 meshed is very small.

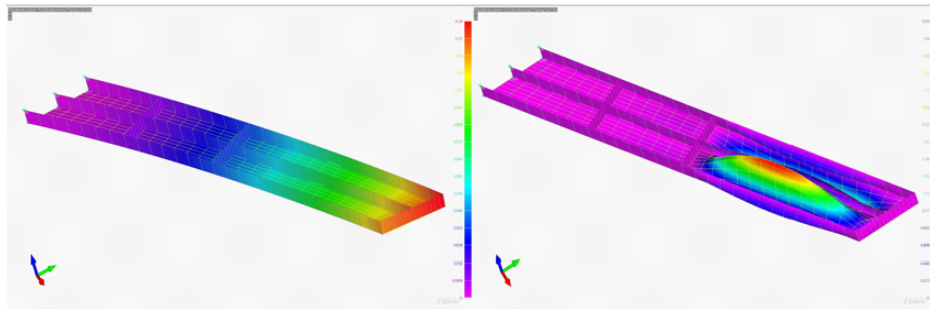


**Fig. 26 Second Swept Wing With Ribs 1, 2, and 4 First Bending and Torsion Modes**

The second swept wing has a torsional moment that is similar to the first swept wing. The main deformation occurs on the trailing edge side between the tip of the wing and meshed rib 2. When comparing the torsional mode from Figure 26, with the previous torsional mode in Figure 23, the deformation in Figure 26 is between the swept wing tip, and node 2, while in Figure 23, the deformation mainly takes place between rib 1 and the tip. Taking a look at both shapes, the addition of rib 2 allows the wing to maintain its shape despite the torsional mode taking place, while in Figure 23, the wing still bends. The elastic bending moment on the other hand remains very similar. The most deformation happens near the wing tip, and as the wing gets closer to the root, the deformation subsides. This shows that the addition meshing rib 2 will not affect the bending moment that much. The modal analysis in Table 11 shows very little difference between modes 1 and 2 going from having only ribs 1 and 4 meshed and comparing to having ribs 1,2 and 4 meshed. When comparing Figures 24, 25, and 26, they all have very similar bending deformations and the movement is about the same. This shows that the shape of the wings, and the implementation of rib 1 does not effect the bending deformation that much. When looking at the torsional deformations, all three wings can maintain their shape and restrict movement during the mode 2 animation. The location of the deformation is also in the same spot for all 3 wings.

#### F. Modal Analysis of Wings With Ribs 1, 2, 3, and 4 Meshed and Imposed Boundary Conditions

For this modal analysis, rib 3 gets meshed. This means that all the wing ribs are meshed, and all other conditions remain the same. The location of rib 3 can be found in Figures 1, 3, and 5 for their respective wings.

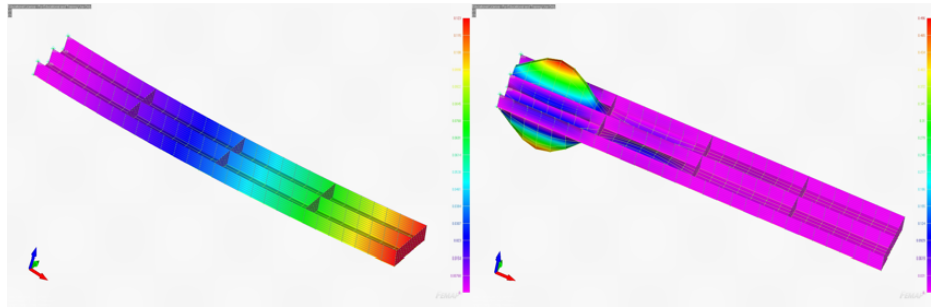


**Fig. 27 Unswept Wing With Ribs 1, 2, 3, and 4 First Bending and Torsion Modes**

With all the ribs now meshed, the unswept wing can be seen as having a maximum torsional deformation near the root of the wing mainly between rib 1 and the root of the wing. The shape of the wing remains the same, and there is very little torsional movement to be seen in mode 2. The bending deformation of the unswept wing shows a maximum deformation at the tip of the wing, and as the wing moves closer to the root, the deformation subsides. When comparing Figure 27 and Figure 24, the torsional deformation is on opposite sides, the straight wing's deformation occurs at the wing root and leading edge, while the deformation of the swept wings occurs at the wing root on the trailing edge side. In Figure 27, the deformation affects a smaller area in comparison to the deformation in Figure 24 and is mainly seen at the root of the wing between the root and rib 1, while in Figure 24, the deformation covers a larger area between the wing tip and rib 2. Both shapes of the wings remain very similar and there is very little movement to be seen due to torsion. The addition of more wing ribs allows the wing to stay more rigid and not be affected by movement due to torsional deformation. The bending deformations between Figure 27, and Figure 24 are very similar. The wing still moves around about the same which further shows that the addition of ribs does not affect the wing movements.

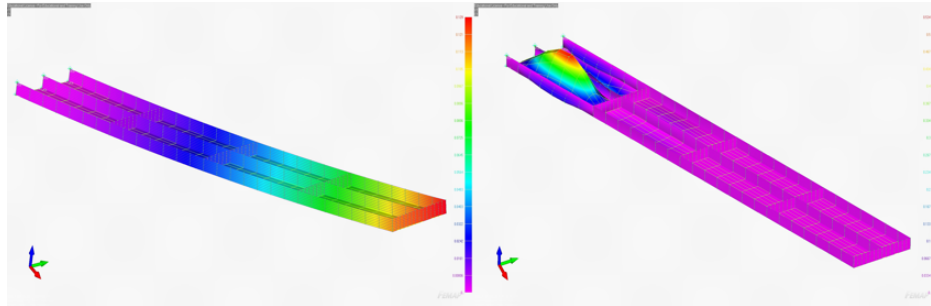


**Fig. 28 First Swept Wing With Ribs 1, 2, 3, and 4 First Bending and Torsion Modes**

The torsional deformation affects the first swept wing near the root of the wing as seen above in figure 28. The shape of the wing does not bend with the addition of rib 3, and there is very little movement to be seen in mode 2. The bending deformation of the wing, on the other hand, affects the wing mainly at the tip of the wing and starts to subside as the wing moves closer to the root. When comparing the torsional deformation between Figure 28, and Figure 25, the addition of meshed rib 3 moves the deformation from being mainly between rib 2 and the tip to now being between the wing root and rib 1. Their shape remains very similar and there is very little movement of the wing affected by torsion. When looking at the bending deformation between Figures 28 and 25, their shape remains very similar. Their shapes both create a similar bend and the deformations are both very similar. The addition of ribs does not affect the bending moments of the wings.

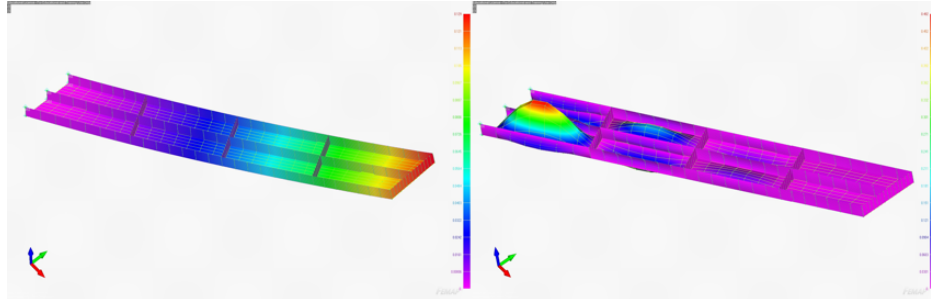


**Fig. 29 Second Swept Wing With Ribs 1, 2, 3, and 4 First Bending and Torsion Modes**

The torsional deformation affects the third swept wing mainly between rib 1 and the root, but there are also some deformations between ribs 1 and 2, and then less between ribs 2 and 3. This shows that the torsional deformation is spread out more throughout the wing not just between the root and wing 1. The shape of the wing remains the same and there is very little torsional movement when looking at mode 2. The elastic deformation on the other hand sees a trend of having a maximum deformation near the wing tip and decreasing as the deformation moves towards the root. The shape shows a clear bend and there is still a movement to be seen in mode 1. When comparing the second swept wing in Figure 29 with Figure 26, the torsional deformation is in 2 different spots. In Figure 26, the deformation only affects the area that is not ribbed between rib 2 and the tip. Whereas in Figure 29, the deformation mainly occurs between the root and rib 1, but it also continues between ribs 1 to rib 3. The shape of both wings is not affected though. When looking at the bending deformation between the two wings, the addition of rib 3 does not affect the shape or the deformation of the wing and they remain very similar.

Taking a look at modes 1 and 2 of the unswept wing as well as both swept wings, there is not much difference to be seen between having rib 3 meshed, and without it. There is a slight decrease that can be seen in Tables 9, 10, and 11, but mainly it remains the same. Comparing the elastic deformations between the three wings in Figures 27, 28, and 29, the shape of the three wings experiences similar bending. The three wings also experience similar deformation that is at its maximum at the wing tip and subsides as the wings move towards the wing root. Comparing all three of their torsional deformations, there are some distinct differences. While the shape of the three wings remains the same, and none of them experience much movement due to torsion, their deformation areas are different. The unswept wing has its main deformation between the wing root and rib 1, but it also experiences some deformation between ribs 1 and 2. The second swept wing on the other hand only has an affected deformation area between the root of the wings and rib 1. The third swept wing has an affected deformation mainly between the wing root and rib 1, but the deformation continues between rib 1 through rib 3. This shows that the different rib geometry does affect the deformation area of the wings.

#### G. Modal Analysis of Wings With Ribs 1, 2, 3, and 4 Meshed without Imposed Boundary Conditions

In this analysis, we were assigned to remove the clamped boundary condition and keep the ribs meshed. We are to compare the difference that this makes between having the boundary condition versus not having the boundary condition. When looking at the first 6 modes, the difference is very drastic. Getting rid of the boundary condition makes the first 6 modes very small, very similar to the modal analysis of the no ribs and no boundary conditions. After that, modes 6 through 10 get very similar with both having the boundary condition and the unbound wings. When comparing the unbound wings that have all the ribs meshed with the unbound wings with no ribs meshed, there is a big difference still between modes 7 through 10. This is mostly due to the unbound wings with no ribs converging only after  $n = 3$  meshing iterations, while the unbound wings with ribs were tested with a mesh of  $n=7$  iterations.

#### H. Overall Analysis of All Rib Configurations

As noted before, the following tables are the modes and frequencies of the wings and their respective rib configuration. Aligning the tables this way allows us to see the trends that come with introducing ribs into the wing structure. As you can see, introducing the ribs steadily increases the modal frequencies. Similarly, this trend has the greatest effect on the second wing geometry, which was the swept wing with the ribs perpendicular to the leading edge. Following this, one could conclude that this geometry would be best structurally when considering the wing structure of a plane.

Modes for all Rib Configurations at (n=7) (Hz)					
Mode	Rib 4	Ribs 1,4	Ribs 1,2,4	All Ribs	All Ribs, No Clamp
1	6.545912	6.546079	6.542019	6.524502	1.21846E-4
2	22.98183	22.98318	22.96774	22.90077	1.09808E-4
3	29.30213	30.84237	31.32313	31.42496	6.88282E-5
4	30.64597	31.99823	32.15074	32.82934	6.47495E-5
5	31.94364	32.34067	32.82935	33.05802	5.59082E-5
6	32.11883	32.8302	32.96901	33.14136	8.798489E-5
7	32.41625	32.93952	33.16655	33.2407	29.19252
8	32.84417	33.59494	34.45917	35.93375	29.60507
9	33.41349	33.80354	35.93392	37.0665	32.81459
10	34.1377	34.9857	36.34208	37.46139	33.05782
11	35.03198	35.94401	36.70696	37.49603	N/A
12	36.11194	36.57706	37.57289	37.94956	N/A
13	36.96886	37.80645	38.46346	38.49115	N/A
14	37.39131	38.44869	38.57825	38.69349	N/A
15	37.99756	38.51039	38.59709	38.73038	N/A

**Table 9 First Wing: 15 Natural Modes and Frequencies for Differing Rib Configurations, Clamped Constraint Condition**

Modes for all Rib Configurations at (n=7) (Hz)					
Mode	Rib 4	Ribs 1,4	Ribs 1,2,4	All Ribs	All Ribs, No Clamp
1	4.914098	4.923651	4.920934	4.907632	1.69259E-5
2	15.55605	15.5556	15.54551	15.50235	4.88118E-5
3	27.25838	27.3664	27.51023	27.64466	5.7881E-5
4	28.96461	36.18627	41.30773	41.82371	7.2419E-5
5	41.19631	41.22378	41.75105	41.9621	1.11217E-4
6	41.28409	41.39579	41.82371	41.97959	1.20542E-4
7	41.43355	41.69786	41.98606	41.99633	22.41365
8	41.65145	41.82399	42.57605	43.88283	28.24702
9	41.94584	42.15299	43.4733	44.72718	41.81253
10	42.327	42.7928	43.8826	44.83931	41.96201
11	42.80612	43.65551	43.89843	44.988	N/A
12	43.39381	43.88636	44.88133	45.4833	N/A
13	44.09624	44.79233	45.85309	46.53295	N/A
14	44.90984	46.22398	46.53294	47.94808	N/A
15	45.23837	46.54134	47.94731	49.20455	N/A

**Table 10 Second Wing: 15 Natural Modes and Frequencies for Differing Rib Configurations, Clamped Constraint Condition**

Modes for all Rib Configurations at (n=7) (Hz)					
Mode	Rib 4	Ribs 1,4	Ribs 1,2,4	All Ribs	All Ribs, No Clamp
1	4.915336	4.924975	4.92884	4.91177	7.54613E-5
2	15.5643	15.56537	15.55791	15.5217	4.49489E-5
3	27.29124	27.42077	27.59131	27.7199	3.76373E-5
4	28.9989	35.97458	41.33489	41.73364	4.80741E-6
5	41.23155	41.25816	41.73333	41.78799	3.45726E-5
6	41.32012	41.4284	41.75536	41.83708	1.40594E-4
7	41.47349	41.71941	41.8259	41.89254	22.3732
8	41.69599	41.74837	42.52644	43.43879	27.72688
9	41.99159	42.16798	43.36132	43.8444	41.72486
10	42.3677	42.772	43.43894	44.09475	41.78727
11	42.83241	43.43625	43.702	44.33784	N/A
12	43.3927	43.60103	44.03786	45.3818	N/A
13	44.05883	44.61344	45.47379	46.31514	N/A
14	44.84437	45.89823	46.31574	47.37454	N/A
15	45.29515	46.34898	47.37403	48.31077	N/A

**Table 11 Third Wing: 15 Natural Modes and Frequencies for Differing Rib Configurations, Clamped Constraint Condition**

## VI. Conclusion

From the FEMAP analysis done on three different wing geometries above, we can make many of the following conclusions. The necessity of ribs is unquestionable as they provide much-needed torsional and bending stiffness to the wing structure. As demonstrated by the slow introduction of each rib, the torsional deformation lessened, and the tip deflection also went down. Similarly, the strongest wing geometry structurally is the swept wing, which displayed the greatest rib effectiveness along its geometry.

## References

- [1] Rao, S. S., and Griffin, P., Mechanical vibrations, Harlow: Pearson, 2018.
- [2] Demasi, Luciano. “AE 410: Aerospace Structural Dynamics Final Project 2023. <https://sdsu.instructure.com/courses/139174/assignments/1111035>, 11 Dec. 2023.

## VII. Appendix

### A. MATLAB Code Unconstrained Wing

```
%%
clc; clear all; close all;

% Santiago Ulloa
% AE 410
%%
--GEO_1_UNconstrained--
--frequency convergence test--
% modes for each n
modes_n1 = [4.55953E-5 ;4.50913E-5 ;3.07425E-5 ;2.38254E-5 ;7.86928E-6 ;
```

```

2.7636E-5 ;8.493468 ;11.25928 ;26.66122 ;48.2544 ;]' ;

modes_n2 = [4.06926E-5 ;2.64363E-5 ;1.51636E-5 ;2.31479E-5 ;3.12995E-5 ;
3.35252E-5 ;10.0955 ;12.43983 ;27.2055 ;27.85394 ;]' ;

modes_n3 = [4.0028E-5 ;3.74877E-5 ;3.62053E-5 ;2.49457E-5 ;2.37732E-5 ;
2.81764E-5 ;10.07182 ;12.48879 ;26.91498 ;28.32136 ;]' ;

% modes = [modes_n1; modes_n2; modes_n3];
modes = [modes_n1; modes_n2]; s = size(modes);s = s(1);
p_modes_12 = abs((modes(s, 7:end)-modes(s-1, 7:end)) ./ modes(s, 7:end)) *
100;
modes = [modes_n2; modes_n3]; s = size(modes);s = s(1);
p_modes_23 = abs((modes(s, 7:end)-modes(s-1, 7:end)) ./ modes(s, 7:end)) *
100;

p12 = mean(p_modes_12, "all");p23 = mean(p_modes_23, "all");
disp('----- GEO 1 UNCONSTRAINED -----')
disp('converge mode shape at n=3, average percent difference bewteen n2 and n3
for the final four modes:')
disp(p23)

figure()
all_p = [p12, p23];
subplot 131
plot(1:2,all_p , '-o'); hold on
plot( 0:3,linspace(1, 1, 4), '--r')
xlim([0 3]); xlabel('Convergence Test Run')
ylim(); ylabel('Convergence Percent Difference (%)')
title('Convergence Test for Unconstrained Unswept Wing')
xticks([1:2]); grid on;
legend('Percent Difference', '')

%%
clear;
%--GEO_2_UNconstrained--
%--frequency convergence test--
% modes for each n
modes_n1 = [2.62964E-5 ;2.06066E-5 ;1.23234E-5 ;1.42125E-5 ;1.95793E-5 ;
3.50034E-5 ;10.07669 ;14.60378 ;29.93033 ;42.5681 ;]' ;

modes_n2 = [1.72246E-5 ;2.08837E-5 ;2.5424E-5 ;2.62982E-5 ;3.44284E-5 ;
5.13055E-5 ;12.21224 ;16.02875 ;23.87261 ;26.05149 ;]' ;

modes_n3 = [6.84555E-5 ;5.29943E-5 ;2.89488E-5 ;2.49445E-5 ;2.602E-5 ;
2.78003E-5 ;12.18326 ;16.095 ;23.74134 ;25.9392 ;]' ;

% modes = [modes_n1; modes_n2; modes_n3];
modes = [modes_n1; modes_n2]; s = size(modes);s = s(1);
p_modes_12 = abs((modes(s, 7:end)-modes(s-1, 7:end)) ./ modes(s, 7:end)) *
100;
modes = [modes_n2; modes_n3]; s = size(modes);s = s(1);
p_modes_23 = abs((modes(s, 7:end)-modes(s-1, 7:end)) ./ modes(s, 7:end)) *
100;

```

```

p12 = mean(p_modes_12, "all");p23 = mean(p_modes_23, "all");
disp('----- GEO 2 UNCONSTRAINED -----')
disp('converge mode shape at n=3, average percent difference bewteen n2 and n3
      for the final four modes:')
disp(p23)

all_p = [p12, p23];
subplot 132
plot(1:2,all_p , '-o')
hold on
plot( 0:3,linspace(1, 1, 4), '--r')
xlim([0 3]); xlabel('Convergence Test Run')
ylim(); ylabel('Convergence Percent Difference (%)')
title('Convergence Test for Unconstrained First Swept Wing')
xticks([1:2]); grid on;
legend('Percent Difference', '')

% figure;
% figure;
% plot(1:15, p_modes, '*')

%%
clear;
---GEO_3_UNconstrained--
---frequency convergence test--
% modes for each n
modes_n1 = [2.62964E-5 ;2.17552E-5 ;1.3684E-5 ;1.54072E-5 ;1.93901E-5 ;
3.39775E-5 ;10.07669 ;14.60378 ;29.93033 ;42.5681 ;]';
modes_n2 = [2.688E-5 ;2.34141E-5 ;1.62339E-5 ;7.72696E-6 ;2.46415E-5 ;
2.77693E-5 ;12.20906 ;16.05532 ;23.93782 ;26.07764 ;]';
modes_n3 = [6.8158E-5 ;2.95635E-5 ;2.54532E-6 ;1.47553E-5 ;2.44916E-5 ;
3.8719E-5 ;12.17815 ;16.1002 ;23.7784 ;25.96442 ;]';

% modes = [modes_n1; modes_n2; modes_n3];
modes = [modes_n1; modes_n2]; s = size(modes);s = s(1);
p_modes_12 = abs((modes(s, 7:end)-modes(s-1, 7:end)) ./ modes(s, 7:end)) *
100;
modes = [modes_n2; modes_n3]; s = size(modes);s = s(1);
p_modes_23 = abs((modes(s, 7:end)-modes(s-1, 7:end)) ./ modes(s, 7:end)) *
100;

p12 = mean(p_modes_12, "all");p23 = mean(p_modes_23, "all");
disp('----- GEO 3 UNCONSTRAINED -----')
disp('converge mode shape at n=3, average percent difference bewteen n2 and n3
      for the final four modes:')
disp(p23)

all_p = [p12, p23];
subplot 133
plot(1:2,all_p , '-o')
hold on

```

```

plot( 0:3,linspace(1, 1, 4), '--r')
xlim([0 3]); xlabel('Convergence Test Run')
ylim(); ylabel('Convergence Percent Difference (%)')
title('Convergence Test for Unconstrained Second Swept Wing')
xticks([1:2]); grid on;
legend('Percent Difference', '')

```

## B. MATLAB Code for Constrained Wing

```

%%
clc; clear all; close all;

% Santiago Ulloa
% AE 410
%--GEO_1_constrained--
%--frequency convergence test--
% modes for each n
modes_n1 = [5.885562 ;12.00704 ;20.65999 ;35.20296 ;100.4713 ;
195.8484 ;855.9577 ;1240.036 ;1606.076 ;1610.18 ;1778.037 ;2245.904 ;
2312.894 ;2382.56 ; 2383.843 ]';

modes_n2 = [6.735366 ;13.13974 ;23.56274 ;27.91435 ;28.77208 ;29.17186 ;
29.63085 ;29.98094 ;30.22797 ;30.24226 ;31.18835 ;31.6161 ;34.98108 ;
35.28616 ;35.68003 ]';

modes_n3 = [6.695903 ;13.09996 ;23.43204 ;29.74191 ;29.82773 ;30.22587 ;
30.54669 ;30.97148 ;31.23715 ;31.36104 ;31.39049 ;31.46976 ;31.56966 ;
31.61291 ;33.94004 ]';

modes_n4 = [5.658896 ;13.08285 ;23.33981 ;31.08064 ;31.21682 ;31.78112 ;
31.78265 ;31.81701 ;31.83908 ;31.89016 ;32.00339 ;32.23497 ;32.67213 ;
33.45091 ; 34.78754 ]';

modes_n5 = [6.633134 ;13.07273 ;23.26793 ;30.87562 ;30.96132 ;31.88895 ;
31.97267 ;32.11846;32.33659 ;32.64236 ;33.0577 ;33.61264 ;34.34686 ;
35.31046 ;36.55698 ]';

modes_n6 = [6.611872 ;13.06566 ;23.20828 ;30.72202 ;30.76568 ;31.92292 ;
32.05697 ;32.286 ;32.61871 ;33.06701 ;33.64618 ;34.37446 ;35.27128 ;36.35375 ;
37.3986]';

modes_n7 = [6.594324 ;13.06024 ;23.15745 ;30.60013 ;30.61177 ;31.94017 ;
32.1046 ;32.38345 ;32.78399 ;33.31556 ;33.98927 ;34.817 ;35.80923 ;
36.97254 ;37.45245 ;]';

modes = [modes_n1; modes_n2]; s = size(modes);s = s(1);
p_modes_12 = abs((modes(s, :)-modes(s-1, :)) ./ modes(s, :)) * 100;
modes = [modes_n2; modes_n3]; s = size(modes);s = s(1);
p_modes_23 = abs((modes(s, :)-modes(s-1, :)) ./ modes(s, :)) * 100;
modes = [modes_n3; modes_n4]; s = size(modes);s = s(1);
p_modes_34 = abs((modes(s, :)-modes(s-1, :)) ./ modes(s, :)) * 100;
modes = [modes_n4; modes_n5]; s = size(modes);s = s(1);
p_modes_45 = abs((modes(s, :)-modes(s-1, :)) ./ modes(s, :)) * 100;
modes = [modes_n5; modes_n6]; s = size(modes);s = s(1);

```

```

p_modes_56 = abs((modes(s, :) - modes(s-1, :)) ./ modes(s, :)) * 100;
modes = [modes_n6; modes_n7]; s = size(modes); s = s(1);
p_modes_67 = abs((modes(s, :) - modes(s-1, :)) ./ modes(s, :)) * 100;

p12 = mean(p_modes_12, "all"); p23 = mean(p_modes_23, "all");
p34 = mean(p_modes_34, "all"); p45 = mean(p_modes_45, "all");
p56 = mean(p_modes_56, "all"); p67 = mean(p_modes_67, "all");

disp('----- GEO 1 CONSTRAINED -----')
disp('converge mode shape at n=7, average percent difference bewteen n6 and n7
      ')
disp(p67)

all_p = [p12, p23, p34, p45, p56, p67];

figure()
subplot 131
plot(1:6, all_p, '-o')
hold on
plot(0:7, linspace(1, 1, 8), '--r')
xlim([0 7]); xlabel('Convergence Test Run')
ylim([0 5]); ylabel('Convergence Percent Difference (%) (%)')
title('Convergence Test for Constrained Unswept Wing')
xticks(1:6); grid on

% figure;
% plot(1:15, p_modes, '*')

%%%
clear;
%--GEO_2_constrained--
%--frequency convergence test--
% modes for each n
modes_n1 = [4.330006 ; 13.66425 ; 14.1005 ; 35.87851 ; 90.59793 ; 168.2364;
1011.674 ;
1486.788 ; 1709.139 ; 1728.547 ; 1896.181 ; 2405.598 ; 2445.149 ;
2570.631 ; 2642.007 ;]';

modes_n2 = [5.031512 ; 15.30699 ; 15.89902 ; 29.59065 ; 31.87972 ; 32.10723 ;
32.16876 ; 33.90804 ; 35.68364 ; 37.03718 ; 37.91389 ; 38.38489 ; 40.10016 ;
40.70202 ; 41.41762 ;]';

modes_n3 = [5.007081 ; 15.27115 ; 15.82114 ; 28.64776 ; 31.09076 ; 34.1243 ;
34.28076 ; 34.96887 ; 35.95972 ; 36.59035 ; 37.09772 ; 37.34857 ; 37.85147 ;
38.14902 ; 38.22206 ;]';

modes_n4 = [4.986999 ; 15.25171 ; 15.76904 ; 28.11112 ; 30.6736 ; 37.96489 ;
38.05416 ; 38.47834 ; 38.49693 ; 38.90608 ; 39.07228 ; 39.46212 ; 39.66187 ;
40.08985 ; 40.32747 ;]';

modes_n5 = [4.971873 ; 15.24034 ; 15.72824 ; 27.77241 ; 30.40412 ; 40.6948 ;
40.70578 ; 40.77319 ; 40.81528 ; 40.86276 ; 40.95397 ; 41.03409 ; 41.06868 ;
41.08658 ; 41.27234 ;]';

```

```

modes_n6 = [4.959551 ;15.2328 ;15.69483 ;27.52434 ;30.21424 ;41.15739 ;
41.1918 ;41.25358 ;41.26383 ;41.3516 ;41.497 ;41.70493 ;41.99253 ;42.37974 ;
42.88026 ;]';

modes_n7 = [4.949234 ;15.22735 ;15.66641 ;27.33083 ;30.06685 ;41.19527 ;
41.24524 ;41.27967 ;41.42307 ;41.63148 ;41.91172 ;42.2721 ;42.72042 ;43.2623 ;
43.89539 ;]';

modes = [modes_n1; modes_n2]; s = size(modes);s = s(1);
p_modes_12 = abs((modes(s, :) - modes(s-1, :)) ./ modes(s, :)) * 100;
modes = [modes_n2; modes_n3]; s = size(modes);s = s(1);
p_modes_23 = abs((modes(s, :) - modes(s-1, :)) ./ modes(s, :)) * 100;
modes = [modes_n3; modes_n4]; s = size(modes);s = s(1);
p_modes_34 = abs((modes(s, :) - modes(s-1, :)) ./ modes(s, :)) * 100;
modes = [modes_n4; modes_n5]; s = size(modes);s = s(1);
p_modes_45 = abs((modes(s, :) - modes(s-1, :)) ./ modes(s, :)) * 100;
modes = [modes_n5; modes_n6]; s = size(modes);s = s(1);
p_modes_56 = abs((modes(s, :) - modes(s-1, :)) ./ modes(s, :)) * 100;
modes = [modes_n6; modes_n7]; s = size(modes);s = s(1);
p_modes_67 = abs((modes(s, :) - modes(s-1, :)) ./ modes(s, :)) * 100;

p12 = mean(p_modes_12, "all");p23 = mean(p_modes_23, "all");
p34 = mean(p_modes_34, "all");p45 = mean(p_modes_45, "all");
p56 = mean(p_modes_56, "all");p67 = mean(p_modes_67, "all");

disp('----- GEO 2 CONSTRAINED -----')
disp('converge mode shape at n=7, average percent difference bewteen n6 and n7
:');
disp(p67)

all_p = [p12, p23, p34, p45, p56, p67];
subplot 132
plot(1:6,all_p , '-o')
hold on
plot( 0:7,linspace(1, 1, 8), '--r')
xlim([0 7]); xlabel('Convergence Test Run')
ylim([0 5]); ylabel('Convergence Percent Difference (%)')
title('Convergence Test for Constrained First Swept Wing')
xticks([1:6]); grid on;

% figure;
% plot(1:15, p_modes, '*')

%%
clear;
%--GEO_3_constrained--
%--frequency convergence test--
% modes for each n
modes_n1 = [4.330006 ;13.66425 ;14.1005 ;35.87851 ;90.59793 ;168.2364 ;
1011.674 ;1486.788 ;1709.139 ;1728.547 ;1896.181 ;2405.598 ;2445.149 ;
2570.631 ;2642.007 ;]';

modes_n2 = [5.036017 ;15.30832 ;15.96366 ;29.84333 ;32.16821 ;32.62669 ;
32.73516 ;34.33269 ;35.99818 ;37.34777 ;38.26054 ;38.78617 ;41.41321 ;

```

```

41.83597 ;41.86525 ;]' ;

modes_n3 = [5.011112 ;15.26884 ;15.85207 ;28.79436 ;31.25027 ;34.21057 ;
34.3515 ;35.11617 ;36.35162 ;36.69324 ;37.49295 ;38.16391 ;38.63196 ;
38.64638 ;39.37983 ;]' ;

modes_n4 = [4.989595 ;15.25032 ;15.78705 ;28.19696 ;30.77036 ;37.69996 ;
37.81542 ;38.43553 ;38.71849 ;38.8199 ;39.19976 ;39.67812 ;40.06863 ;
40.07362 ;40.18525 ;]' ;

modes_n5 = [4.973695 ;15.23927 ;15.74083 ;27.82898 ;30.4742 ;40.68978 ;
40.73798 ;40.85062 ;40.88396 ;40.94088 ;40.96484 ;41.04297 ;41.10965 ;
41.15674 ;41.19178 ;]' ;

modes_n6 = [4.960802 ;15.23201 ;15.70423 ;27.56239 ;30.2661 ;41.20472 ;
41.23983 ;41.27265 ;41.30699 ;41.4116 ;41.5582 ;41.75719 ;42.01731 ;
42.34725 ;42.76022 ;]' ;

modes_n7 = [4.950135 ;15.22677 ;15.67386 ;27.3579 ;30.10727 ;41.23008 ;
41.2521 ;41.31406 ;41.45962 ;41.67016 ;41.94807 ;42.29935 ;42.7286 ;
43.24024 ;43.84098 ;]' ;

modes = [modes_n1; modes_n2]; s = size(modes);s = s(1);
p_modes_12 = abs((modes(s, :)-modes(s-1, :)) ./ modes(s, :)) * 100;
modes = [modes_n2; modes_n3]; s = size(modes);s = s(1);
p_modes_23 = abs((modes(s, :)-modes(s-1, :)) ./ modes(s, :)) * 100;
modes = [modes_n3; modes_n4]; s = size(modes);s = s(1);
p_modes_34 = abs((modes(s, :)-modes(s-1, :)) ./ modes(s, :)) * 100;
modes = [modes_n4; modes_n5]; s = size(modes);s = s(1);
p_modes_45 = abs((modes(s, :)-modes(s-1, :)) ./ modes(s, :)) * 100;
modes = [modes_n5; modes_n6]; s = size(modes);s = s(1);
p_modes_56 = abs((modes(s, :)-modes(s-1, :)) ./ modes(s, :)) * 100;
modes = [modes_n6; modes_n7]; s = size(modes);s = s(1);
p_modes_67 = abs((modes(s, :)-modes(s-1, :)) ./ modes(s, :)) * 100;

p12 = mean(p_modes_12, "all");p23 = mean(p_modes_23, "all");
p34 = mean(p_modes_34, "all");p45 = mean(p_modes_45, "all");
p56 = mean(p_modes_56, "all");p67 = mean(p_modes_67, "all");

disp('----- GEO 3 CONSTRAINED -----')
disp('converge mode shape at n=7, average percent difference bewteen n6 and n7
:');
disp(p67)

all_p = [p12, p23, p34, p45, p56, p67];
subplot 133
plot(1:6,all_p , '-o')
hold on
plot( 0:7,linspace(1, 1, 8), '--r')
xlim([0 7]); xlabel('Convergence Test Run')
ylim([0 5]); ylabel('Convergence Percent Difference (%)')
title('Convergence Test for Constrained Second Swept Wing')
xticks([1:6]); grid on;

```